

Bioinspired Catalytic Reduction of Aqueous Perchlorate by One Single-Metal Site with High Stability against Oxidative Deactivation

Changxu Ren and Jinyong Liu*



Cite This: *ACS Catal.* 2021, 11, 6715–6725



Read Online

ACCESS |



Metrics & More



Article Recommendations



Supporting Information

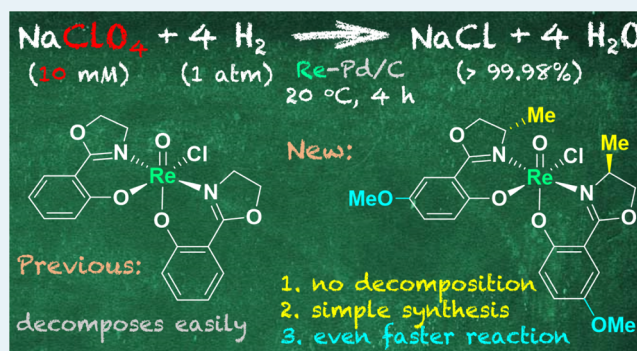
ABSTRACT: Reduction of perchlorate (ClO_4^-) with an active and stable catalyst is of great importance for environmental, energy, and space technologies. However, after the rate-limiting oxygen atom transfer (OAT) from inert ClO_4^- , the much more reactive ClO_x^- ($x \leq 3$) intermediates can cause catalyst deactivation. The previous Re-Pd/C catalyst contained a $[\text{Re}^{\text{V}}(\text{O})(\text{hoz})_2]^+$ site ($\text{Hhoz} = 2-(2'-\text{hydroxyphenyl})-2\text{-oxazoline}$) and readily reduced ClO_4^- , but ClO_x^- intermediates led to rapid formation and hydrolysis of $[\text{Re}^{\text{VII}}(\text{O})_2(\text{hoz})_2]^+$. While microbes use delicate enzymatic machinery to survive the oxidative stress during ClO_4^- reduction, a synthetic catalyst needs a straightforward self-protective design. In this work, we introduced a methyl group on the ligand oxazoline moiety and achieved a substantial enhancement of catalyst stability without sacrificing the performance of ClO_4^- reduction. A suite of kinetics measurement, X-ray photoelectron spectroscopy characterization, reaction modeling, stopped-flow photospectrometry, and ^1H NMR monitoring revealed the underlying mechanism. The most critical and unexpected effect of the methyl group is the deceleration (for 2 orders of magnitude) of OAT from ClO_3^- to $[\text{Re}^{\text{V}}(\text{O})(\text{Mehoz})_2]^+$. However, the rate of OAT with ClO_4^- was not affected. The methyl group also slowed down the hydrolysis of $[\text{Re}^{\text{VII}}(\text{O})_2(\text{Mehoz})_2]^+$ and allowed the introduction of methoxy onto the phenolate moiety to further accelerate ClO_4^- reduction. With 1 atm H_2 at 20 °C, the Re-Pd/C catalyst used $[\text{Re}^{\text{V}}(\text{O})(\text{MehozOMe})_2]^+$ as the only reaction site to reduce multiple spikes of 10 mM ClO_4^- into Cl^- without decomposition. This work showcases the significant effect of simple ligand modification in improving catalyst stability for high-performance ClO_4^- reduction.

KEYWORDS: perchlorate reduction, catalyst stability, rhenium, ligand modification, oxygen atom transfer, hydrolysis, oxidative deactivation

INTRODUCTION

Over the past two decades, perchlorate (ClO_4^-) has increasingly drawn public attention as a pervasive and persistent water pollutant due to the improper disposal of energetic materials and natural atmospheric formation.^{1–4} Because excess exposure to ClO_4^- can cause thyroid malfunction,⁵ many states in the U.S. have set the limits for ClO_4^- at 0.8–18 $\mu\text{g L}^{-1}$ in drinking water.^{3,6} The interest in ClO_4^- has been further stimulated by the recent discovery of ClO_4^- on Mars,^{7–10} moon,¹¹ and meteorites,^{11,12} which collectively imply its wide distribution throughout (and perhaps beyond) the solar system.^{11,13} Thus, the reduction and utilization of ClO_4^- have considerable importance for human's extraterrestrial exploration by removing chemical hazard, improving soil habitability, providing life support, and fueling vehicle operations.¹⁴

While ClO_4^- is highly inert under ambient conditions, microorganisms have developed delicate enzymatic machinery for ClO_4^- reduction (Figure 1a). The sequential $2e^-$ reduction of ClO_4^- to ClO_3^- and ClO_2^- are fulfilled by (per)chlorate



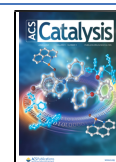
reductase, which contains a molybdopterin-coordinated Mo cofactor as the active site.¹⁵ A series of Fe–S clusters, heme complexes, and electron shuttle compounds enable the electron transfer and redox cycling of the Mo cofactor.^{16–18} The further reduction of ClO_2^- in the same pathway will generate highly reactive HClO/ClO^- ($\text{p}K_a$ 7.5), which can irreversibly inactivate the enzyme by reacting with both the metal factors and the protein.¹⁹ Thus, a second enzyme, chlorite dismutase, uses a heme factor to convert ClO_2^- into innocuous Cl^- and O_2 .²⁰ However, ClO^- can still be released from approximately 1 out of 100 reaction cycles.¹⁹ Another defense mechanism against ClO^- is realized by a methionine-rich periplasmic protein.²¹ The oxidized sulfoxide product is

reductase, which contains a molybdopterin-coordinated Mo cofactor as the active site.¹⁵ A series of Fe–S clusters, heme complexes, and electron shuttle compounds enable the electron transfer and redox cycling of the Mo cofactor.^{16–18} The further reduction of ClO_2^- in the same pathway will generate highly reactive HClO/ClO^- ($\text{p}K_a$ 7.5), which can irreversibly inactivate the enzyme by reacting with both the metal factors and the protein.¹⁹ Thus, a second enzyme, chlorite dismutase, uses a heme factor to convert ClO_2^- into innocuous Cl^- and O_2 .²⁰ However, ClO^- can still be released from approximately 1 out of 100 reaction cycles.¹⁹ Another defense mechanism against ClO^- is realized by a methionine-rich periplasmic protein.²¹ The oxidized sulfoxide product is

Received: December 2, 2020

Revised: May 10, 2021

Published: May 24, 2021



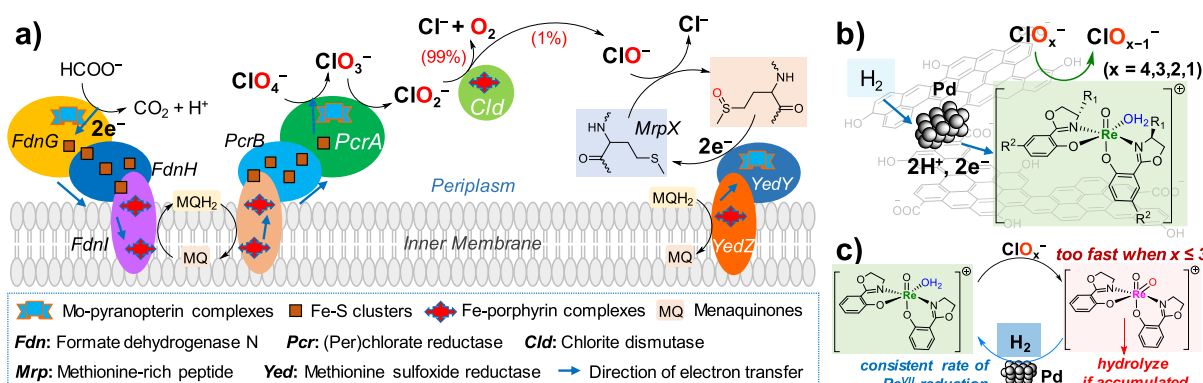


Figure 1. (a) Overall microbial reduction of ClO_4^- including electron harvest from organic donors, (per)chlorate reduction, chlorite dismutation, and hypochlorite scavenging; (b) simplified bioinspired design of Re–Pd/C; and (c) mechanistic challenge of the previous catalyst.

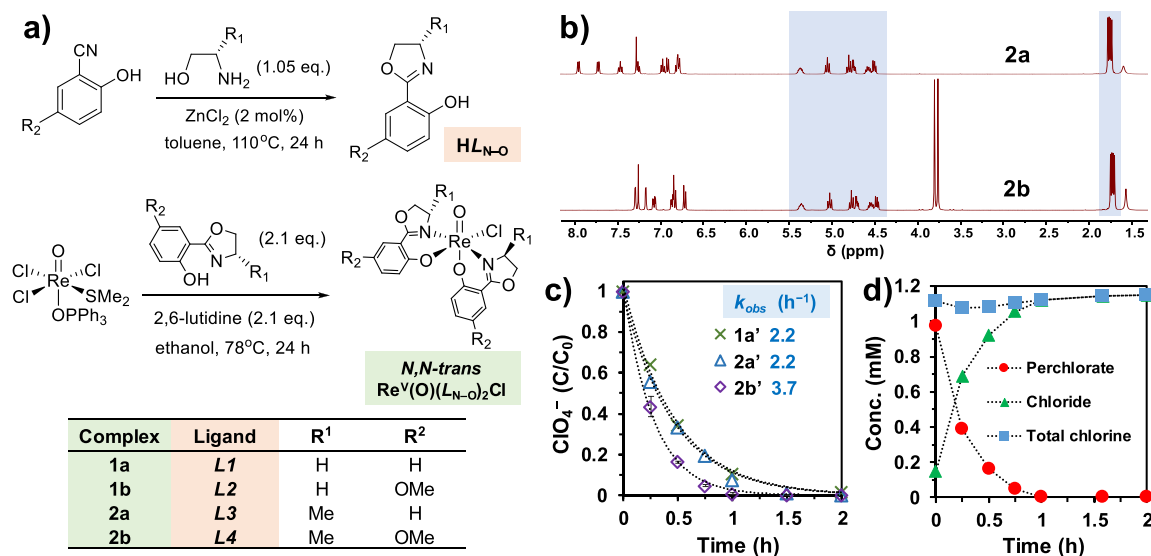


Figure 2. (a) Synthesis of $\text{HL}_{\text{N-O}}$ ligands and $\text{Re}^{\text{V}}(\text{O})(\text{L}_{\text{N-O}})_2\text{Cl}$ complexes; (b) comparison of ^1H NMR spectra for 2a^{33} and 2b with signals of the two 4-methyloxazoline moieties highlighted in blue; (c) degradation profile of 1 mM ClO_4^- by Re–Pd/C catalysts (0.5 g L^{-1} , 5 wt % Re and 5 wt % Pd, pH 3.0, 1 atm H_2 , 20 °C); and (d) chlorine balance using the Re–Pd/C prepared from 2b .

regenerated by a methionine sulfoxide reductase that uses a Mo cofactor.²² Therefore, the rapid and robust microbial reduction of ClO_4^- is achieved through the cooperation of all components and functions.²³

Significant efforts have been taken to design synthetic metal catalysts that mimic biochemical principles to reduce ClO_4^- and other oxyanions.^{24–30} In particular, we have developed a bioinspired Re–Pd/C catalyst, in which the single-site $[\text{Re}^{\text{V}}(\text{O})(\text{hoz})_2]^+$ complex ($\text{Hoz} = 2-(2'-\text{hydroxyphenyl})-2\text{-oxazoline}$), Pd^0 nanoparticles with H_2 gas, and the porous carbon (Figure 1b) mimic the three essential components of the enzyme system, the Mo cofactor, the electron transfer chain, and the protein support.²⁸ While homogeneous metal catalysts are moisture-sensitive^{24,29,30} or require special electron donors such as hydrazine, ferrocene, sulfide, and phosphine,^{24–26} the heterogeneous Re–Pd/C platform enables rapid reduction of aqueous ClO_4^- by 1 atm H_2 at 20 °C.²⁸ However, upon rapid oxidation by the highly reactive ClO_x^- intermediates, accumulated $[\text{Re}^{\text{VII}}(\text{O})_2(\text{hoz})_2]^+$ in the $\text{Re}^{\text{V/VII}}$ cycle is subject to irreversible hydrolysis (Figure 1c).³¹ Because simplicity is essential for both bioinspired design and practical application, the multicomponent defense mechanism used by microbes cannot be readily mimicked in a synthetic catalyst

system. Therefore, a novel “self-defense” mechanism for the Re site against oxidative deactivation is of great interest to both catalytic science and engineering. In other words, can we develop a single-metal site that is both active and stable without a multicomponent protection mechanism? If yes, how simple is the design of such a metal site?

In this contribution, we report on the discovery and elucidation of a surprising and advantageous structure-stability feature. Without lowering the rate of ClO_4^- reduction, the introduction of a methyl group to the original *hoz* ligand substantially slowed down (1) the oxidation of the Re^{V} site by ClO_x^- intermediates and (2) the hydrolysis of the Re^{VII} site. The “evolved” catalyst exhibited high stability against oxidative deactivation and thus significantly enhanced the performance in ClO_4^- reduction. This simple ligand modification provided effective protection of the reactive site, demonstrating a novel strategy to design catalysts with a single-metal site against deactivation by reaction intermediates.

RESULTS AND DISCUSSION

Catalyst Preparation and Basic Performance. To interrogate the effects of ligand structure modification on catalyst performance, we synthesized new N,O-bidentate

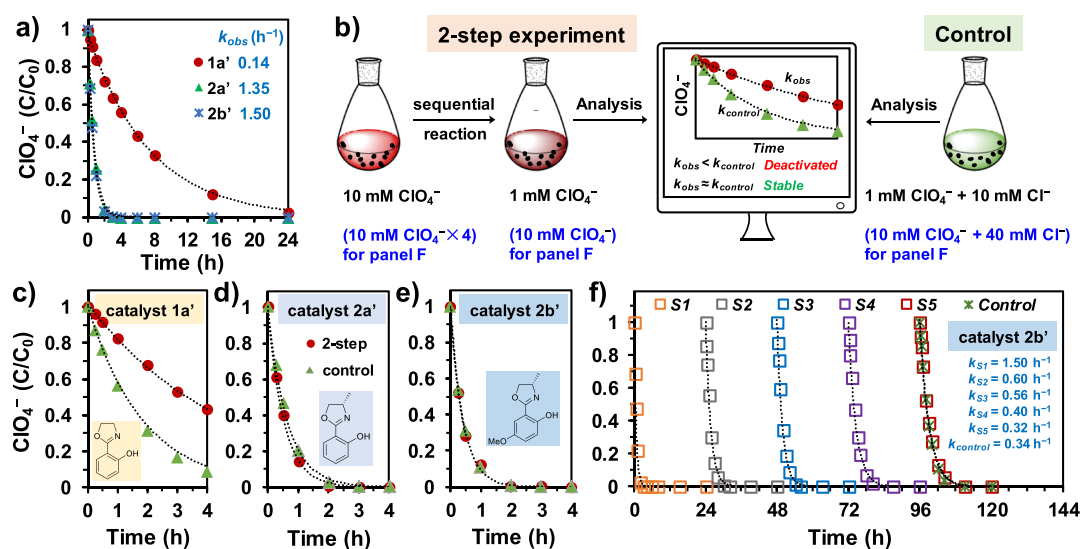


Figure 3. (a) Degradation profile of 10 mM ClO₄⁻ by Re–Pd/C catalysts (0.5 g L⁻¹, 5 wt % Re and 5 wt % Pd, pH 3.0, 1 atm H₂, 20 °C); (b) illustration of the two-step stability test and the control experiment; (c–e) results of the stability test showing the effect of the L_{N–O} structure (the common legend is in panel d); and (f) stability challenge of catalyst 2b' with five spikes of 10 mM ClO₄⁻.

ligands (HL_{N–O}) derived from the original *Hhoz* ligand (HL1, Figure 2a). The oxazolinyphenolate structure is naturally occurring in microbial siderophores.³² The HL_{N–O} ligands were synthesized *via* one-step construction of the oxazoline ring from specific benzonitriles and amino alcohols. The Re^V(O)(L_{N–O})₂Cl complexes were prepared with our established method³³ and used as the precursor for Re–Pd/C catalysts. Detailed procedures are described in Experimental Section of the Supporting Information.

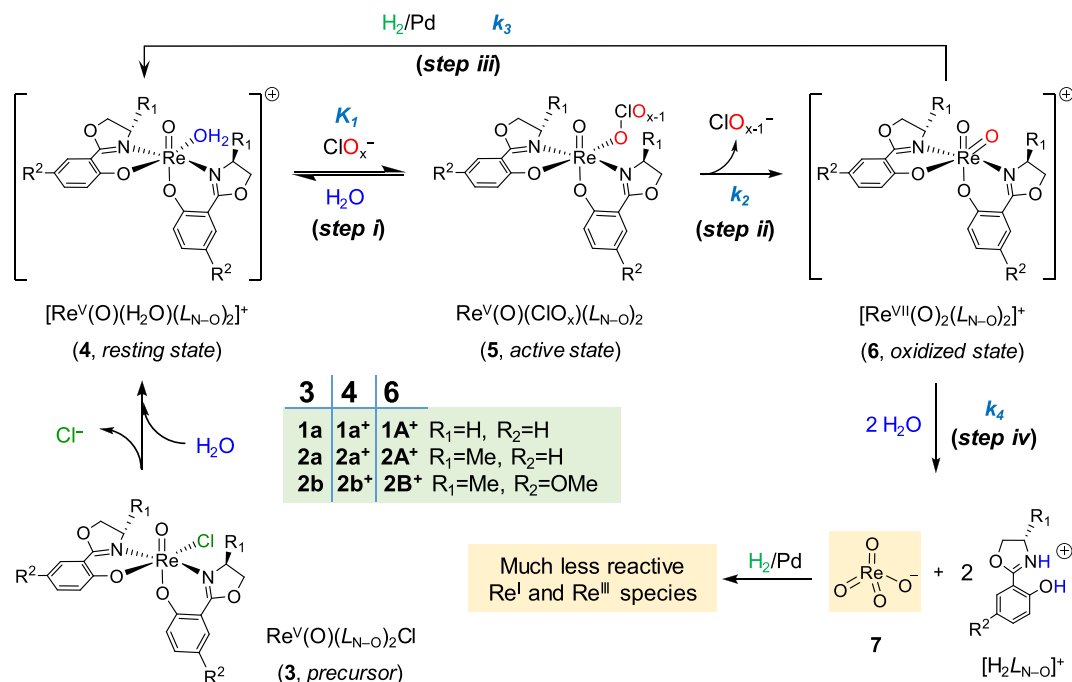
To enhance the reactivity of Re^V with ClO₄⁻, we first introduced an electron-donating –OMe to the phenol moiety of *Hhoz* (L2). However, the synthesis of Re^V(O)(L2)₂Cl (1b) yielded a mixture of two products with poor solubility in most solvents, preventing further isolation and characterization. To increase the solubility and restrict the isomerization,²⁷ we introduced a methyl group on the oxazoline moiety (L3 and L4) by switching the amino alcohol building block from glycylol to *L*-alaninol.³³ The corresponding Re^V(O)(L_{N–O})₂Cl products (2a and 2b) showed good solubilities in dichloromethane and chloroform. Comparison of ¹H NMR spectra with the previously characterized 2a (Figure 2b, δ 4.0–5.5 for H's on the oxazoline ring and δ 1.7 for H's of the methyl group) confirmed the exclusive yield of *N,N*-*trans* Re^V(O)-(L_{N–O})₂Cl.³³ Single crystallography of 2b (Figure S1, not refined due to high-level disorders) also confirmed the *N,N*-*trans* configuration. For comparison, the original L1 led to the formation of both *N,N*-*cis* and *N,N*-*trans* Re^V(O)(*hoz*)₂Cl (1a). Previous studies have confirmed that *N,N*-*cis* isomers are much less active than the *N,N*-*trans* counterparts for ClO₄⁻ reduction.²⁷ Therefore, the use of the minimally steric –Me on the oxazoline moiety mimics the biochemical replacement of glycine with alanine and ensures the exclusive formation of the desirable *N,N*-*trans* Re complexes.

To evaluate the activity and stability of Re–Pd/C catalysts (labeled 1a', 2a', and 2b'), we immobilized the corresponding Re^V(O)(L_{N–O})₂Cl precursors (1a, 2a, and 2b) in Pd/C with an aqueous deposition method.²⁸ Briefly, the powders of the Re complex and Pd/C were sonicated and stirred in water suspension under 1 atm H₂. The transiently dissolved Re complex in water was adsorbed into porous carbon and

immobilized by hydrophobic and electrostatic interactions.²⁸ We observed >95% of Cl⁻ in all three precursors released in water, indicating a near-complete immobilization and activation of Re for the reduction of aqueous ClO₄⁻.²⁸ All Re–Pd/C catalysts exhibited a rapid reduction of 1 mM ClO₄⁻ by 1 atm H₂ at 20 °C (Figure 2c). The –Me substitution on oxazoline did not alter the rate of ClO₄⁻ reduction (1a' vs 2a'). The –OMe substitution provided a 68% faster ClO₄⁻ reduction (2b' vs 2a'). As the oxygen atom transfer (OAT) from ClO₄⁻ to Re^V decreases the electron density of Re, an electron-rich ligand can promote this process.³⁴ The chlorine balance was closed by ClO₄⁻ and Cl⁻ (Figure 2d). The initial 0.13 mM Cl⁻ was released from the precursor 2b (0.134 mM was added). More than 99.99% of 1 mM ClO₄⁻ was completely reduced to Cl⁻ within 1 h. The turnover number (TON) on each Re site was 7.5 for the reduction of ClO₄⁻ (or 30 if all four oxygen atoms were abstracted by the same OAT mechanism). The absence of a hydrogen-bonding motif (*e.g.*, amino acid residues in enzymes¹³ or the secondary coordination sphere in an artificial Fe complex²⁴) for the metal-bound oxanion required a slightly acidic environment (*e.g.*, pH 3.0) to enable OAT.^{28,35}

Before we further discuss the kinetics, we note that the heterogeneous nature of Re–Pd/C catalysts has been confirmed in previous studies.^{28,31} The direct use of Re complex 1a²⁸ or 2b did not show ClO₄⁻ reduction in the pure aqueous medium (Figure S2) for two reasons: (1) the solubility of Re(O)(L)₂Cl in water is low and (2) the Re(O)(L)₂Cl precursor cannot spontaneously release the chloro ligand to allow the coordination with ClO₄⁻. The hydrophobic and electrostatic interactions between the Re complex and carbon surface provide unique advantages for the heterogeneous system. When cationic 1a⁺ and 2a⁺ (the Cl⁻ in 1a and 2a was removed by AgOTf) were dissolved in acetonitrile for homogeneous LiClO₄ reduction by alkyl sulfides, 2a⁺ was quickly inhibited by the Cl⁻ from ClO₄⁻ reduction, whereas the activity of 1a⁺ sustained longer (Figure S3). Product inhibition by Cl⁻ was also observed from a homogeneous Fe catalyst.^{24,25} In stark comparison, 1a' and 2a' showed almost identical activity (Figure 2c). The immobilized

Scheme 1. Proposed Transformation of Molecular Re Species at the Carbon–Water Interface



Re complexes interact more strongly with the carbon surface than with aqueous Cl^- . During the aqueous deposition process, >95% of Cl^- in $\text{Re}^{\text{V}}(\text{O})(\text{L}_{\text{N-O}})_2\text{Cl}$ precursors were expelled into the aqueous phase. Compared to the high sensitivity of $[\text{Re}^{\text{V}}(\text{O})(\text{L}_{\text{N-O}})_2]^+$ with Cl^- in the acetonitrile solution, the 0.13 mM Re in Re–Pd/C catalysts was only partially inhibited even in the presence of 10–50 mM Cl^- (*vide infra*).

Catalyst Stability against Oxidative Deactivation. While the higher activity of $2\text{b}'$ than $1\text{a}'$ was expected, to our surprise, $2\text{b}'$ exhibited high stability against oxidative deactivation. For the reduction of 1 mM ClO_4^- , the apparent first-order rate constant by $2\text{b}'$ was 68% higher than that by $1\text{a}'$ (Figure 2c). However, the rate constants for 10 mM ClO_4^- (TON = 75 for ClO_4^- or 300 for abstracting all four oxygen atoms) by $2\text{a}'$ and $2\text{b}'$ were 8.6- and 9.7-fold higher than that by $1\text{a}'$, respectively (Figure 3a). This significant difference in reducing concentrated ClO_4^- implies that the Re site in $2\text{a}'$ and $2\text{b}'$ is much more stable than that in $1\text{a}'$.

We systematically assessed the catalyst stability by conducting two sets of kinetic experiments (Figure 3b). In the first set, each Re–Pd/C catalyst was used to reduce 10 mM ClO_4^- for 24 h, so that even the least active $1\text{a}'$ could complete the reduction (Figure 3a). To probe whether the Re sites were still active, we added another spike of 1 mM ClO_4^- to the used catalysts and measured the reduction kinetics. Because the generation of 10 mM Cl^- can slightly inhibit the Re–Pd/C catalyst by competing with ClO_4^- for the reactive site,³¹ in the second set of control experiments, we measured the reduction of 1 mM ClO_4^- by freshly prepared Re–Pd/C catalysts in the presence of 10 mM NaCl (mimicking the generation of Cl^- from 10 mM ClO_4^-). The significant disparity between the two experiments for $1\text{a}'$ (Figure 3c) suggests a major deactivation of Re sites during the reduction of 10 mM ClO_4^- . In stark contrast, $2\text{a}'$ and $2\text{b}'$ showed a negligible difference between the two experiments (Figure 3d,e). Hence, the reduction of 10 mM ClO_4^- by $2\text{a}'$ and $2\text{b}'$ did not lead to a noticeable activity loss. For a single batch of 10 mM ClO_4^- ,

>97 and >99.98% reduction were achieved by $2\text{b}'$ within 2 h and 4 h, respectively. The initial turnover frequency (TOF₀) calculated from the reduction of the first 5% of 10 mM ClO_4^- was 109 h⁻¹ (or 436 h⁻¹ for abstracting all four oxygen atoms, see the Supporting Information for the method of TOF₀ calculation).

The high stability of catalyst $2\text{b}'$ was further verified by reusing it for reducing five spikes of 10 mM ClO_4^- (Figure 3f). Each ClO_4^- spike was completely reduced using 24 h before the next spike. The kinetics of the fifth spike was almost the same as the control experiment, where freshly prepared $2\text{b}'$ reduced 10 mM ClO_4^- in the presence of 40 mM NaCl (mimicking the four earlier ClO_4^- spikes). Hence, the gradual decrease in catalyst activity was solely attributed to the significant buildup of Cl^- in the water. This high stability makes $2\text{b}'$ the most active catalyst for aqueous ClO_4^- reduction among all chemical reduction systems reported to date (Tables S1 and S2).^{34,36–44}

As elucidated in previous studies, the OAT from ClO_x^- oxidizes $[\text{Re}^{\text{V}}(\text{O})(\text{L}_{\text{N-O}})_2]^+$ into $[\text{Re}^{\text{VII}}(\text{O})_2(\text{L}_{\text{N-O}})_2]^+$ (steps i and ii in Scheme 1).^{28,45} Organic sulfide (in the homogeneous system) or Pd-activated H_2 (in the heterogeneous system) removes one oxo group and thus reduces Re^{VII} back to Re^{V} (step iii). If the oxidation is faster than the reduction, the accumulated $[\text{Re}^{\text{VII}}(\text{O})_2(\text{L}_{\text{N-O}})_2]^+$ is subject to hydrolytic decomposition into $\text{Re}^{\text{VII}}\text{O}_4^-$ and $[\text{H}_2\text{L}_{\text{N-O}}]^+$ (step iv).³¹ Because ClO_4^- is much more inert than ClO_x^- intermediates, we attributed the catalyst deactivation to the highly reactive ClO_3^- , ClO_2^- , and ClO^- intermediates. When the initial concentration of ClO_4^- was elevated, the concentrations of ClO_x^- intermediates from the first-order reduction of ClO_4^- were also proportionally elevated, thus imposing higher oxidative “stress” to the Re sites. To confirm this mechanistic insight, we further challenged Re–Pd/C catalysts by directly exposing them to ClO_3^- (Figure 4a). The one-time addition of 0.5–1.0 mM ClO_3^- imposed substantially higher oxidative stress than the gradual generation (accompanied with rapid

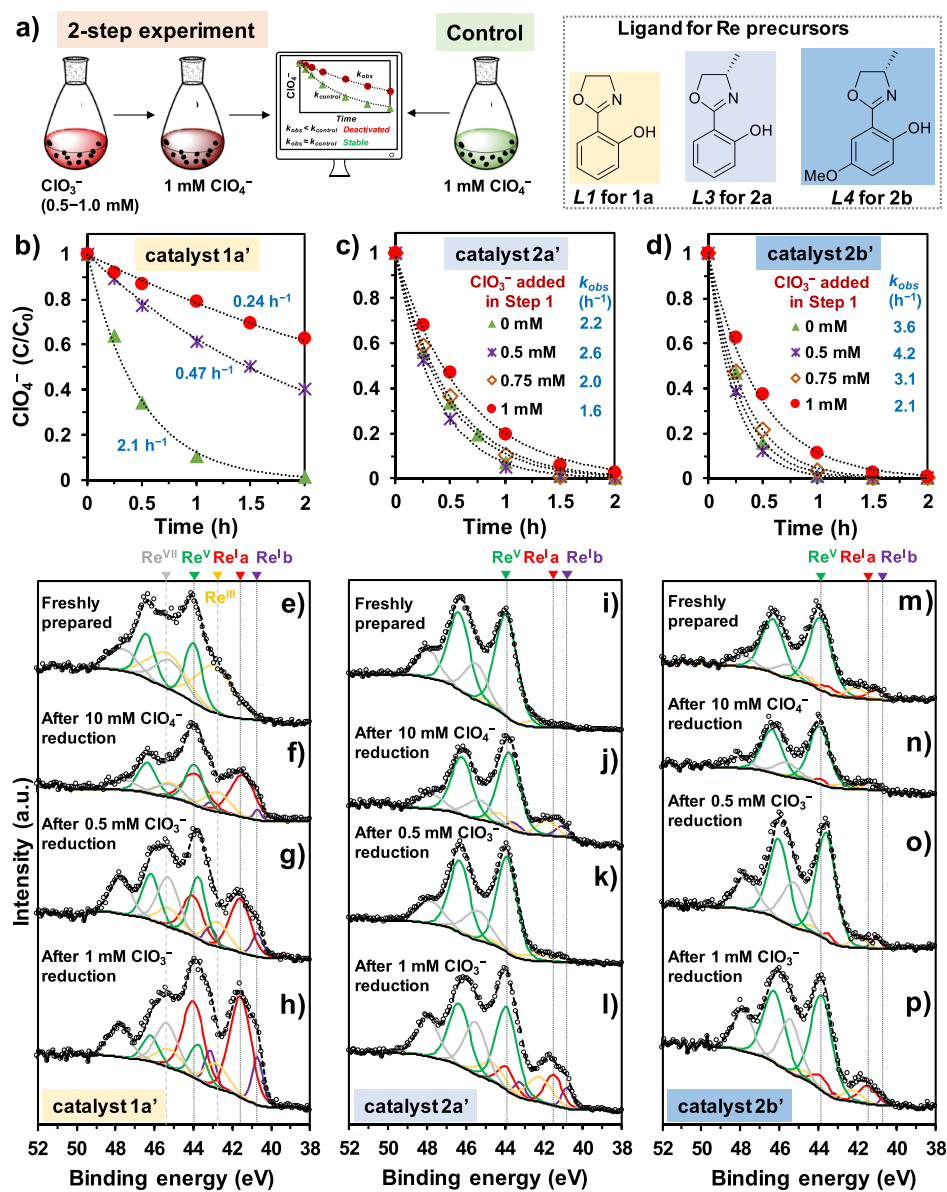


Figure 4. (a) Illustration of the two-step stability test using ClO_3^- and the control experiment; (b–d) results of the stability tests (the common legend is shown in panels c or d, 0.5 g L^{-1} of 5 wt % Re and 5 wt % Pd, pH 3.0, 1 atm H_2 , 20°C); and (e–p) Re 4f XPS spectra of the three catalysts under various conditions. The Re $4f_{7/2}$ peaks are highlighted with dotted lines.

degradation) of ClO_3^- from the pseudo-first-order decay of 10 mM ClO_4^- . As shown in Figure 4c,d, the one-time addition of 0.5 mM ClO_3^- did not deactivate catalyst 2a' and 2b' in the following reduction of 1 mM ClO_4^- . When ClO_3^- was increased to 1 mM, we observed deactivation to a limited extent. In stark comparison, 1a' was severely deactivated by 0.5 and 1 mM ClO_3^- (Figure 4b).

We used X-ray photoelectron spectroscopy (XPS) to probe the evolution of Re speciation in the Re–Pd/C catalysts after use under various conditions. The fresh catalyst 1a' contained three Re species with $4f_{7/2}$ binding energies of 42.8 eV, 44.0 eV, and 45.2 eV (Figure 4e), which are consistent with reported Re^{III} , Re^{V} , and Re^{VII} , respectively.²⁸ The detection of Re^{III} was attributed to the reduction of the oxo group in $[\text{Re}^{\text{V}}(\text{O})(\text{L}_{\text{N-O}})_2]^+$ by Pd-activated H_2 (heterogeneous) or by PPh_3 (homogeneous).²⁸ Interestingly, 2a' and 2b' contained little Re^{III} (Figure 4i,m), probably due to the steric effect of methyl groups in L3 and L4. However, this difference did not

cause different catalytic activities by 1a' and 2a' (Figure 2c). The detection of Re^{VII} is caused by the trace amount of O_2 during the sample preparation and transfer (see Supporting Information, Experimental Section). After the reduction of 10 mM ClO_4^- , two new Re $4f_{7/2}$ peaks at 40.7 eV and 41.6 eV showed up in 1a' (Figure 4f). To understand these two species, we prepared the ReO_x –Pd/C catalyst from KReO_4 with the same aqueous deposition method.²⁸ The ClO_4^- reduction activity of this catalyst (Figure 5a) was 150- and 257-fold lower than 1a' and 2b', respectively. The $\text{Re}^{\text{VII}}\text{O}_4^-$ is reductively immobilized into low-valent ReO_x species.^{46–48} The XPS spectrum of ReO_x –Pd/C contained a minor peak for Re^{III} (42.6 eV) and two major peaks at 40.8 eV and 41.7 eV (Figure 5b), which have been identified as two different Re^{I} structures.^{47,49} Thus, the two new peaks found in Figure 4f confirmed the decomposition of active Re sites into $\text{Re}^{\text{VII}}\text{O}_4^-$ and the subsequent reduction into Re^{I} . The two Re^{I} species took 42% of the total immobilized Re (Table S3). The XPS

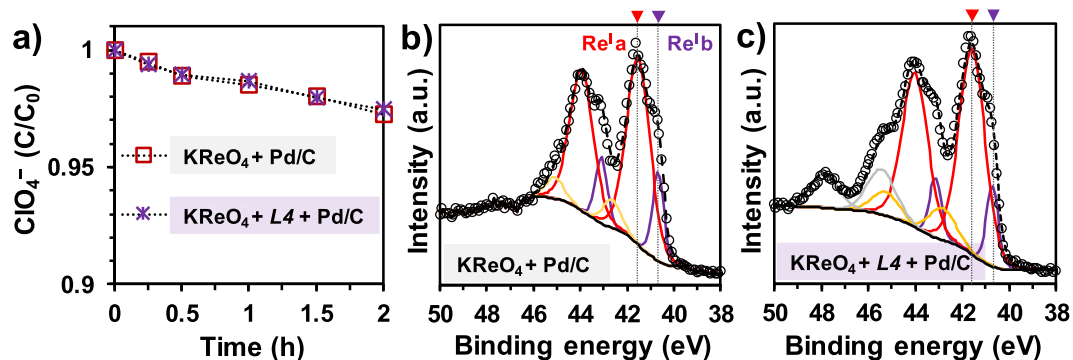


Figure 5. (a) Reduction of 1 mM ClO_4^- by Re–Pd/C catalysts prepared from KReO_4 with and without *L4* and (b + c) Re 4f XPS spectra of the two as-prepared catalysts. Reaction conditions: 0.5 g L^{-1} of 5 wt % Re and 5 wt % Pd, molar ratio of *L4*:Re = 2:1, pH 3.0, 1 atm H_2 , 20 °C. Note the y-axis in panel a starts from $C/C_0 = 0.9$.

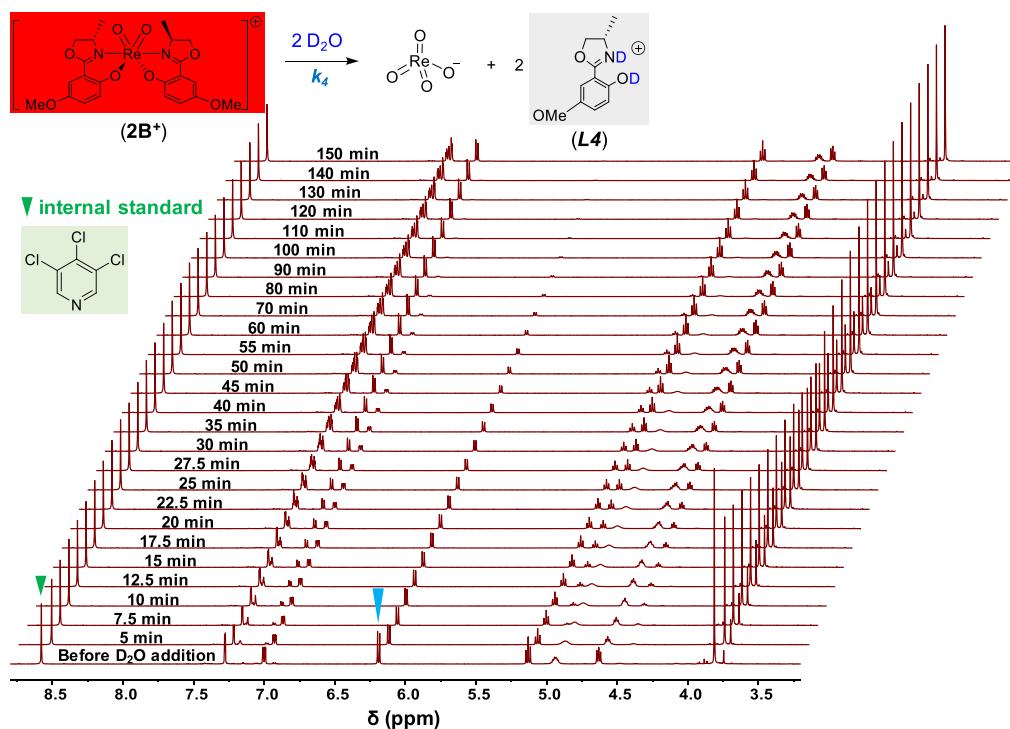


Figure 6. Time-dependent ^1H NMR (600 MHz) spectra for the hydrolysis of 2B^+ (10 mM) in 5/95 (v/v) $\text{D}_2\text{O}/\text{CD}_3\text{CN}$ at 20 °C. The resonance indicated by the blue arrow was used for quantitation shown in Figure 7a.

spectra after reducing 0.5 and 1.0 mM ClO_3^- also showed the two Re^{I} species, taking 35% and 56% of the total Re, respectively (Figure 4g,h and Table S3). Therefore, direct exposure to ClO_3^- caused more severe damage to the active Re sites than treating concentrated ClO_4^- . Moreover, the decomposition of Re sites into $\text{Re}^{\text{VII}}\text{O}_4^-$ and free $\text{L}_{\text{N-O}}$ is a permanent deactivation because the use of $\text{Re}^{\text{VII}}\text{O}_4^-$ and *L4* (the ligand for 2b) did not yield a higher activity than $\text{ReO}_x\text{-Pd/C}$ (Figure 5a). The Re speciation was also similar to $\text{ReO}_x\text{-Pd/C}$ but very different from $2\text{b}'$ (Figures 5c vs 5b and vs 4m–p). This aspect also shows that during the catalyst preparation and normal catalysis, the $\text{Re}(\text{L}_{\text{N-O}})_2$ complex remained intact rather than undergoing “dissociation and reassembly” of Re metal and free $\text{L}_{\text{N-O}}$ ligands on the carbon surface.

In stark contrast, the surface Re speciation in catalysts $2\text{a}'$ and $2\text{b}'$ did not show a meaningful increase in Re^{I} species after reducing either 10 mM ClO_4^- or 0.5 mM ClO_3^- (Figure 4i–p

and Table S3). A small increase in Re^{I} species was observed after the reaction with 1 mM ClO_3^- (Figure 4l,p and Table S3). Thus, XPS characterization results are consistent with the kinetic data shown in Figure 4b–d, providing spectroscopic evidence for the high stability of Re sites in $2\text{a}'$ and $2\text{b}'$. We did not further test ClO_2^- or ClO^- as the more challenging substrates because their side reactions in acidic media⁵⁰ may complicate the analysis and understanding. Moreover, the stepwise reduction from ClO_4^- is less likely to accumulate ClO_2^- or ClO^- in high concentrations.

Mechanisms for the Enhanced Catalyst Stability.

Based on Scheme 1, we developed a quasi-steady-state equation to model the rate of removing $\text{Re}(\text{L}_{\text{N-O}})_2$ sites from the catalytic cycle into decomposition (eq 1, detailed derivation steps provided in Text S1)

$$\frac{d[6]}{dt} = -\frac{nK_1k_2k_4}{k_3}[\text{XO}_n][\text{Re}]_T \quad (1)$$

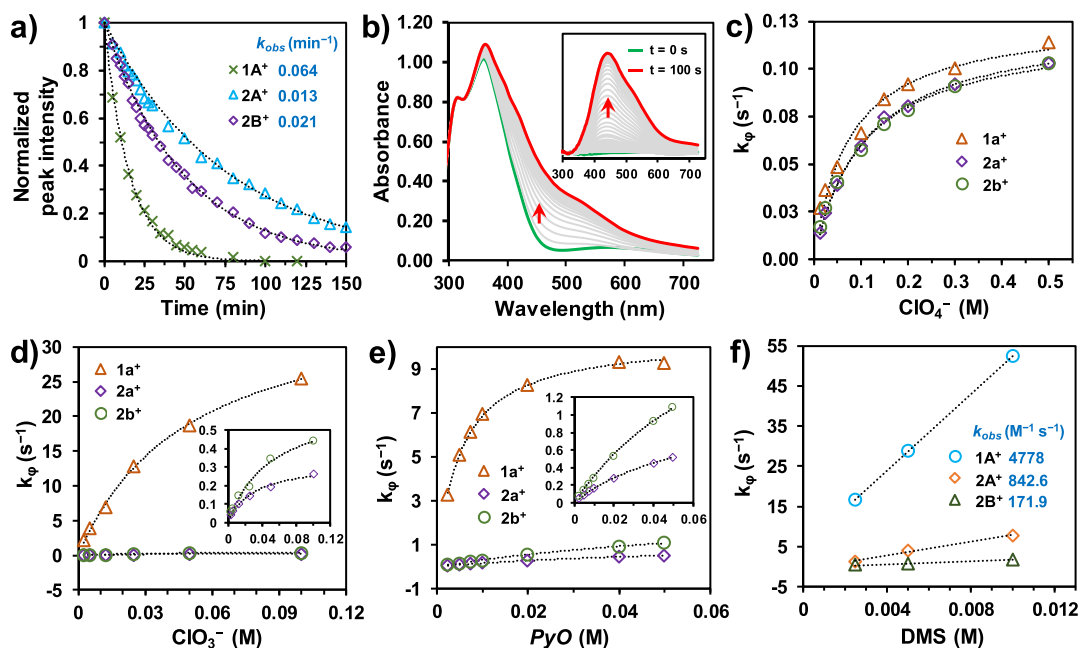


Figure 7. (a) Time profiles of ¹H NMR measured hydrolytic decomposition of $[\text{Re}^{\text{VII}}(\text{O})_2(\text{L}_{\text{N-O}})_2]^+$ in 5/95 (v/v) $\text{D}_2\text{O}/\text{CD}_3\text{CN}$ at 20 °C and (b) time-dependent UV–vis absorption spectra for $1\text{a}^+ \rightarrow 1\text{A}^+$ upon stopped-flow mixing of 0.5 mM 1a^+ and 25 mM LiClO_4 at 1:1 (v/v). Both species were dissolved in anhydrous CH_3CN . The inset shows the change in absorption after subtracting the initial spectrum ($t = 0$ s) from all spectra and (c–f) dependence of the initial rate constant (k_{ϕ}) on the concentrations of ClO_4^- , ClO_3^- , and PyO (for Re^{V} oxidation) and of DMS (for Re^{VII} reduction).

The apparent decomposition rate of the active $\text{Re}(\text{L}_{\text{N-O}})_2$ site is dependent on three reactions: the formation (K_1k_2), reduction (k_3), and hydrolysis (k_4) of $[\text{Re}^{\text{VII}}(\text{O})_2(\text{L}_{\text{N-O}})_2]^+$ (**6**). Because the Re –Pd/C catalysts **1a'** and **2b'** showed surprisingly different stabilities, we expected that the rate constants of one or more steps were significantly altered by the minor modifications of the ligand with $-\text{Me}$ on the oxazoline or $-\text{OMe}$ on the phenolate.

Hydrolytic Decomposition of $[\text{Re}^{\text{VII}}(\text{O})_2(\text{L}_{\text{N-O}})_2]^+$. We first hypothesized that the rate of hydrolysis for **6** (k_4) determines the lifetime of $\text{Re}(\text{L}_{\text{N-O}})_2$ sites. A slow step iv could preserve **6** in the catalytic cycle (Scheme 1). Due to the difficulty of directly probing and modeling molecular transformations at the heterogeneous water–carbon interface, we investigated the hydrolysis of various **6** (**1A⁺**, **2A⁺**, and **2B⁺**) in organic solutions by ¹H NMR (Figures 6, S4, and S5). The solutions of **6** were prepared by sequentially treating the $\text{Re}^{\text{V}}(\text{O})(\text{L}_{\text{N-O}})_2\text{Cl}$ precursor **3** (**1a**, **2a**, and **2b**) with 1 equivalent of AgOTf and 0.25 equivalent of LiClO_4 in a dry box. In anhydrous CD_3CN , **6** was stable for at least 3 days. The ¹H NMR spectra showed symmetry for the two $\text{L}_{\text{N-O}}$ ligands. Based on the reported crystal structures of similar dioxo Re^{VII} complexes,^{45,51} we postulate a C_2 -symmetric *cis*-dioxo configuration for $[\text{Re}^{\text{VII}}(\text{O})_2(\text{L}_{\text{N-O}})_2]^+$ structures in this study. Although the reported crystal structure of $[\text{Re}^{\text{V}}(\text{O})(\text{H}_2\text{O})(\text{L}_{\text{N-O}})_2]^+$ (**4**) has the H_2O *trans* to the oxo group,⁵² it is reasonable to assume that during the rapid catalytic cycles, both H_2O and ClO_x^- coordinate with the Re^{V} center from the equatorial site *cis* to the oxo.²⁷ To normalize the peak intensities of the time-dependent spectra, we used 3,4,5-trichloropyridine as an internal standard ($\delta = 8.6$ ppm).⁵³ The addition of 5% (v/v) D_2O initiated the first-order hydrolysis of **6** (Figure 7a) directly into $\text{Re}^{\text{VII}}\text{O}_4^-$ and double-protonated free ligand $[\text{H}_2\text{L}_{\text{N-O}}]^+$.³¹ Other intermediate structures, such as the previously reported $\text{Re}^{\text{VII}}(\text{O})_3(\text{L}_{\text{N-O}})$,²⁶ were not observed.

The rate constants of hydrolysis for **2A⁺** and **2B⁺** were merely 20% and 33% of that for **1A⁺** (Figure 7a). Thus, the $-\text{Me}$ substitution on oxazoline significantly slowed down the hydrolysis. The faster decomposition of **2B⁺** than **2A⁺** is probably attributed to the increased electron density at the phenolate O, which facilitates the protonation of $\text{L}_{\text{N-O}}$ and detachment from the metal.^{54,55} Although a slower hydrolytic step iv can, to some extent, help preserve **6** in the catalytic cycle, the modestly different rates of hydrolysis for the three structures may not be fully responsible for the markedly different catalyst stability (Figures 3c–e and 4b–d).

Generation of $[\text{Re}^{\text{VII}}(\text{O})_2(\text{L}_{\text{N-O}})_2]^+$ Via OAT Oxidations.

We measured the kinetics of the formation of **6** from the corresponding **4** (dissolved in acetonitrile) via OAT from ClO_4^- , ClO_3^- , and pyridine *N*-oxide (PyO). In anhydrous acetonitrile, **1a⁺** and **2a⁺** exhibit very similar dark green color, whereas **2b⁺** shows a dark brown color (Figure S6). Because all three Re complexes have the same *N,N*-*trans* coordination structure, the absorption red shift of **2b⁺** is attributed to the extended conjugation by $-\text{OMe}$ substitution on the phenolate moiety.^{56,57} We performed oxidation of **4** with excess oxidants under pseudo-first-order conditions and monitored the fast kinetics with stopped-flow spectrophotometry.⁴⁵ After the addition of oxidants, all solutions turned into red color²⁶ due to the increased absorption of 380–700 nm (Figure 7b). The maximum increase in absorbance from **4** to **6** ($\lambda_{\text{max}} = 440$ nm for $1\text{a}^+ \rightarrow 1\text{A}^+$ and $2\text{a}^+ \rightarrow 2\text{A}^+$ and 510 nm for $2\text{b}^+ \rightarrow 2\text{B}^+$) were determined by subtracting the initial absorption spectra of **4** (Figures 7b inset and S7). The representative time profiles for the absorbance at λ_{max} are shown in Figure S7d. The initial rate constant (k_{ϕ}) from such profiles at varied concentrations of ClO_4^- , ClO_3^- , and PyO are shown in Figure 7c–e. All data sets showed the gradual saturation of kinetics as the oxidant concentrations increased.⁴⁵

To model the oxidation of **4** to **6** (steps i and ii in Scheme 1) measured by the stopped-flow experiment, we developed the nonsteady-state eq 2 (detailed derivation steps provided in Text S2)

$$\frac{d[6]}{dt} = \frac{nK_1k_2[XO_n][Re]_T}{1 + K_1[XO_n]} \quad (2)$$

Nonlinear-least-squares fitting of the initial rate data to eq 2 provided the constants K_1 and k_2 for individual oxidants and Re complexes (Table 1). The equilibrium constants for step i

Table 1. Best Fitted Rate Constants from the Data in Figure 7c–e with eq 2

entry	oxygen donor (XO)	K_1 (M^{-1})	k_2 (s^{-1})	$\frac{K_1k_2}{(M^{-1}s^{-1})}$
1a⁺ (from L1)				
1	ClO ₄ [−]	13.2 ± 2.1	0.032 ± 0.004	0.4
2	ClO ₃ [−]	19.7 ± 1.8	12.75 ± 0.670	251.2
3	PyO	191.0 ± 7.2	10.43 ± 0.306	1992.1
2a⁺ (from L3)				
4	ClO ₄ [−]	9.2 ± 0.4	0.031 ± 0.001	0.3
5	ClO ₃ [−]	33.2 ± 8.3	0.109 ± 0.018	3.6
6	PyO	17.3 ± 0.4	1.107 ± 0.009	19.2
2b⁺ (from L4)				
7	ClO ₄ [−]	9.8 ± 0.9	0.030 ± 0.002	0.3
8	ClO ₃ [−]	20.1 ± 4.6	0.219 ± 0.029	4.4
9	PyO	12.1 ± 0.6	2.859 ± 0.092	34.6

(K_1 , for ligand exchange from the solvent to the oxygen donor) depend on both the oxidant and L_{N-O} structure. Among the three oxidants, ClO₄[−] showed the lowest K_1 . This result is consistent with the well-known weak coordinating capability of ClO₄[−].⁵⁸ The substantially lower K_1 for PyO by **2a⁺** and **2b⁺** (17.3 and 12.1 M^{-1}) than by **1a⁺** (191 M^{-1}) is attributed to the steric hindrance by the methyl group on the ligands. The K_1 for ClO₄[−] with **1a⁺** (13.2 M^{-1}) is also slightly higher than that with **2a⁺** and **2b⁺** (9.2 and 9.8 M^{-1}).

For step ii, the three complexes showed very similar k_2 for the OAT from coordinated ClO₄[−] to Re^V (0.030–0.032 s^{-1}). However, to our surprise, the OAT from coordinated ClO₃[−] to **1a⁺** (12.75 s^{-1}) was 2 orders of magnitude faster than to **2a⁺** (0.109 s^{-1}). For the reaction with ClO₃[−], the overall second-order rate constants (K_1k_2) for **2a⁺** and **2b⁺** (3.6 and 4.4 $M^{-1}s^{-1}$) were 70- and 57-fold smaller than for **1a⁺** (251.2 $M^{-1}s^{-1}$, entries 2, 5, and 8 in Table 1). On the basis of eq 1, the substantially slower formation of **6** is beneficial for its stability. We expected similar trends for the even more reactive ClO₂[−] and ClO[−] substrates, but experimental attempts were not successful due to (1) the low solubility of NaClO₂ in pure or water-mixed acetonitrile and (2) uncontrolled reactivity of HClO/ClO[−] with common organics. Hence, we used pyridine

oxide (PyO) as a highly reactive surrogate (entries 3, 6, and 9 in Table 1). For the OAT from PyO to Re^V, the k_2 for **1a⁺** (10.43 M^{-1}) was 1 order of magnitude higher than for **2a⁺** (1.107 M^{-1}). Therefore, the introduction of −Me on the oxazoline moiety of L_{N-O} not only causes a steric hindrance for Re^V to coordinate with the oxygen donor (e.g., PyO) but also slows down the OAT from the coordinated donor (e.g., ClO₃[−] and PyO) to Re^V. The comparison between **2a⁺** and **2b⁺** shows that the −OMe on the phenolate moiety can both decrease K_1 and increase k_2 for ClO₃[−] and PyO but not for ClO₄[−] (entries 4–6 vs 7–9 in Table 1).

Notably, the profiles for the oxidation from **4** to **6** by ClO₃[−] contained two phases with different reaction rates (Figure S8). The fast oxidation in the first phase took only about 0.2 s for **1a⁺**, 15 s for **2a⁺**, and 12 s for **2b⁺**. The much slower oxidation in the second phase took >30 s for **1a⁺**, >300 s for **2a⁺**, and >150 s for **2b⁺**. Both phases exhibited first-order kinetics. A detailed analysis of the time-evolved absorption spectra found the formation of Re^V(O)(L_{N-O})₂Cl (the precursor **3** in Scheme 1), which is responsible for the relatively slow reaction in the second phase. The reduction of highly reactive ClO₃[−] rapidly generates Cl[−], which inhibited the reaction by competing for the coordination site on Re^V (cf. Figure S3). In the homogeneous system, the Re–Cl binding in **2a** is much stronger than in **1a**. Spectroscopic evidence and reasoning are provided in Figures S9–S11. Such two-phase kinetics was less pronounced using the much more inert ClO₄[−] and was not observed from the reaction with PyO.

Reduction of [Re^{VII}(O)₂(L_{N-O})₂]⁺. Because it is challenging to measure redox transformations of Re in the three-phase system of H₂+Pd/C in water, we measured homogeneous reduction of **6** to **4** with dimethyl sulfide (DMS) as the reductant. In a sequential mixing flow circuit, the two solutions containing **4** and PyO (equal molar concentration in anhydrous acetonitrile) were first mixed for a preset aging time to ensure complete oxidation of **4** into **6**. The reduction was initiated by the subsequent mixing with excess DMS. The dependence of the reaction rate constants on DMS concentration is shown in Figure 7f. The second-order rate constants were obtained as the slopes of the linear fittings. The reduction of **2A⁺** (842.6 $M^{-1}s^{-1}$) was 82% slower than that of **1A⁺** (4778 $M^{-1}s^{-1}$). This is probably caused by the steric repulsion⁵² between the ligand methyl group and DMS. We note that in the Re–Pd/C catalyst, Pd-activated hydrogen is much less steric demanding than DMS. However, similar to the 2 orders of magnitude different reactivity of oxidative OAT from coordinated ClO₃[−] to Re^V (Table 1, k_2 of entry 2 vs 5), it is also possible that the −Me substitution decreased the intrinsic reactivity of reductive OAT from Re^{VII} to sulfide. The comparison between **2A⁺** and **2B⁺** indicates the electron-donating effect of the −OMe substitution. The reduction of

Table 2. Rate Constants of All Steps Shown in Scheme 1 and Estimated Decomposition Rate Constants for eq 1

Re precursor	$4K_1k_2$ (ClO ₄ [−]) ($M^{-1}s^{-1}$) ^a	$3K_1k_2$ (ClO ₃ [−]) ($M^{-1}s^{-1}$) ^a	k_3 ($M^{-1}s^{-1}$) ^b	k_4 ($M^{-1}s^{-1}$) ^c	k_{dec} (ClO ₄ [−]) ($M^{-1}s^{-1}$)	k_{dec} (ClO ₃ [−]) ($M^{-1}s^{-1}$)
1a (from L2)	1.6	753.6	4778	3.9×10^{-4}	1.3×10^{-7}	6.0×10^{-5}
2a (from L3)	1.2	10.8	842.6	7.9×10^{-5}	1.1×10^{-7}	1.0×10^{-6}
2b (from L4)	1.2	13.2	171.9	1.3×10^{-4}	8.8×10^{-7}	9.6×10^{-6}

^aMeasurement of K_1 in acetonitrile solution involved ligand exchange with CH₃CN rather than with H₂O. ^bThe reductant was DMS and might have steric hindrance with the ligand methyl groups in **2a** and **2b**. ^cSecond-order rate constants derived from the first-order k_{obs} for hydrolysis shown in Figure 7a. The molar concentration of D₂O in the 5:95 (v/v) D₂O/CD₃CN mixture is approximately 2.8 M.

the more electron-rich $2\mathbf{B}^+$ is slower than that of $2\mathbf{A}^+$ by 80% (171.9 vs 842.6 $\text{M}^{-1} \text{s}^{-1}$).

Overall Stability of $[\text{Re}^{\text{VII}}(\text{O})_2(\text{L}_{\text{N-O}})_2]^+$. The rate constants obtained above allow a quantitative comparison of the decomposition rates for $\mathbf{6}$ with eq 1. Table 2 shows the apparent rate constants, $k_{\text{dec}} = nK_1k_2k_4/k_3$, when the substrate is ClO_4^- ($n = 4$) and ClO_3^- ($n = 3$). For each Re complex, $k_{\text{dec,ClO}_4^-}$ is 1–3 orders of magnitude lower than $k_{\text{dec,ClO}_3^-}$, indicating that the oxidative stress mainly comes from the highly reactive ClO_x^- intermediates. The methyl group on the ligand oxazoline moiety slows down the oxidation (K_1k_2) by ClO_3^- for 2 orders of magnitude, while the rate of oxidation by ClO_4^- was not significantly changed (see Table 1 for uncertainties of the model-fit values). We postulate that the rate constants of the reduction step (k_3) measured using Me_2S could be impacted by the steric repulsion. When Pd-activated H_2 is the reductant, although the magnitude of rate constants are expected to be lower than using Me_2S , it is possible that k_3 for $\mathbf{2a}$ reaches the same order-of-magnitude as that for $\mathbf{1a}$ (i.e., about fivefold higher). In such a case, k_{dec} for $\mathbf{2a}$ and $\mathbf{2b}$ could be further lowered for about fivefold, resulting in much higher catalyst stability than $\mathbf{1a}$. Although $\mathbf{2b}$ exhibited a slower reduction and faster hydrolysis than $\mathbf{2a}$ due to the electronic effect from $-\text{OMe}$ substitution, $\mathbf{2b}'$ already showed high stability after treating five spikes of 10 mM ClO_4^- (Figure 3f). Therefore, the methyl group on the ligand oxazoline moiety played a critical role in protecting the Re site from decomposition. It even allowed $-\text{OMe}$ substitution for a limited enhancement of the apparent rate of aqueous ClO_4^- reduction ($\mathbf{2b}'$ vs $\mathbf{2a}'$ in Figures 2c and 3a). Due to the introduction of the methyl group, the relatively limited detrimental effects from the $-\text{OMe}$ substitution, such as 64% faster hydrolysis (k_4) and 80% slower reduction (k_3 , $\mathbf{2b}$ vs $\mathbf{2a}$ in Table 2), did not cause catalyst decomposition during the reduction of 10 mM ClO_4^- or 0.5 mM ClO_3^- . Although technical challenges prevented us from measuring K_1 and k_2 for the reactions with ClO_2^- and ClO^- , we expect the trends to be similar to the observations using ClO_3^- and PyO . Moreover, the generation of ClO_2^- and ClO^- will not cause significant deactivation of $\mathbf{2b}$. The OAT reduction of ClO_3^- (i.e., the generation of ClO_2^-) has already been slowed down for 2 orders of magnitude by the ligand methyl group (Table 1).

CONCLUSIONS

When a bioinspired catalyst system can reduce the highly inert ClO_4^- , the oxidative deactivation by the much more reactive ClO_x^- intermediates can be a major challenge to the reactive metal sites. Our results show that a simple ligand modification provided multiple benefits to the catalyst development. The methyl group on the oxazoline moiety led to an exclusive formation of N,N -trans $\text{Re}^{\text{V}}(\text{O})(\text{L}_{\text{N-O}})_2\text{Cl}$ precursors and protected the $\text{Re}(\text{L}_{\text{N-O}})_2$ site from decomposition after treating multiple spikes of concentrated ClO_4^- (10 mM or 1 g L^{-1}). In comparison to the original $\text{L}_{\text{N-O}}$ ligand, the added methyl group decelerated the OAT from ClO_3^- to $\text{Re}^{\text{V}}(\text{L}_{\text{N-O}})_2$ for 2 orders of magnitude and the hydrolysis of $\text{Re}^{\text{VII}}(\text{L}_{\text{N-O}})_2$ for several folds. Since the rate of OAT from ClO_4^- to $\text{Re}^{\text{V}}(\text{L}_{\text{N-O}})_2$ was not impacted, the apparent rate for aqueous ClO_4^- reduction by the Re–Pd/C catalyst was not lowered. For comparison, the methoxy substitution on the phenolate moiety slightly enhanced the OAT and hydrolysis steps, but these effects were outweighed by the effects of the methyl group on the oxazoline moiety. Overall, the simple ligand

modification with a methyl group significantly enhanced the stability of the Re site without sacrificing the rate of ClO_4^- reduction.

Unlike the biological system that uses delicate enzymatic machinery to work against the oxidative stress from ClO_x^- intermediates, a bioinspired catalyst system relies on simplicity and self-sustainability. The self-protection mechanism empowers the catalyst to treat concentrated ClO_4^- solutions using a single metal center, thus greatly simplifying the catalyst design and preparation. We anticipate the mechanistic insights and design strategy to benefit the development of a wider scope of catalytic systems, where the deactivation by reaction intermediates is limiting the overall TON and catalyst life.

ASSOCIATED CONTENT

Supporting Information

The Supporting Information is available free of charge at <https://pubs.acs.org/doi/10.1021/acscatal.0c05276>.

Experimental section for Re complex synthesis and characterization, heterogeneous perchlorate reduction, water sample analyses, TOF₀ calculation, XPS characterization, kinetic measurements with ¹H NMR and stopped flow spectrophotometry; additional data for reaction kinetics and XPS characterization; comparison with other perchlorate reduction systems; and derivation of kinetic eqs 1 and 2 (PDF)

AUTHOR INFORMATION

Corresponding Author

Jinyong Liu – Department of Chemical and Environmental Engineering, University of California, Riverside, California 92521, United States; orcid.org/0000-0003-1473-5377; Email: jinyongli@ucr.edu, jinyong.liu101@gmail.com

Author

Changxu Ren – Department of Chemical and Environmental Engineering, University of California, Riverside, California 92521, United States; orcid.org/0000-0002-1109-794X

Complete contact information is available at: <https://pubs.acs.org/doi/10.1021/acscatal.0c05276>

Notes

The authors declare no competing financial interest.

ACKNOWLEDGMENTS

Financial support was provided by the UCR faculty research startup grant, the National Science Foundation (CHE-1709719), and the Strategic Environmental Research and Development Program (ER19-1228). Dr. Ich Tran is acknowledged for assistance in XPS characterization performed at the UC Irvine Materials Research Institute (IMRI) using instrumentation funded in part by the National Science Foundation Major Research Instrumentation Program under grant CHE-1338173.

REFERENCES

- (1) Motzer, W. E. Perchlorate: Problems, detection, and solutions. *Environ. Forensics* **2001**, *2*, 301–311.
- (2) Brandhuber, P.; Clark, S.; Morley, K. A review of perchlorate occurrence in public drinking water systems. *J. Am. Water Works Assoc.* **2009**, *101*, 63–73.

- (3) Kucharzyk, K. H.; Crawford, R. L.; Cosens, B.; Hess, T. F. Development of drinking water standards for perchlorate in the United States. *J. Environ. Manage.* **2009**, *91*, 303–310.
- (4) Cao, F.; Jaunat, J.; Sturchio, N.; Cancès, B.; Morvan, X.; Devos, A.; Barbin, V.; Ollivier, P. Worldwide occurrence and origin of perchlorate ion in waters: A review. *Sci. Total Environ.* **2019**, *661*, 737–749.
- (5) Greer, M. A.; Goodman, G.; Pleus, R. C.; Greer, S. E. Health effects assessment for environmental perchlorate contamination: The dose response for inhibition of thyroidal radioiodine uptake in humans. *Environ. Health Perspect.* **2002**, *110*, 927–937.
- (6) EPA. *Steps Water Systems Can Take to Address Perchlorate in Drinking Water*; (EPA-815-F-20-001); U.S. Environmental Protection Agency, Office of Ground Water and Drinking Water, 2020.
- (7) Hecht, M. H.; Kounaves, S. P.; Quinn, R. C.; West, S. J.; Young, S. M. M.; Ming, D. W.; Catling, D. C.; Clark, B. C.; Boynton, W. V.; Hoffman, J.; DeFlores, L. P.; Gospodinova, K.; Kapit, J.; Smith, P. H. Detection of perchlorate and the soluble chemistry of martian soil at the Phoenix lander site. *Science* **2009**, *325*, 64–67.
- (8) Ming, D. W.; Archer, P. D.; Glavin, D. P.; Eigenbrode, J. L.; Franz, H. B.; Sutter, B.; Brunner, A. E.; Stern, J. C.; Freissinet, C.; McAdam, A. C.; Mahaffy, P. R.; Cabane, M.; Coll, P.; Campbell, J. L.; Atreya, S. K.; Niles, P. B.; Bell, J. F.; Bish, D. L.; Brinckerhoff, W. B.; Buch, A.; Conrad, P. G.; Des Marais, D. J.; Ehlmann, B. L.; Fairén, A. G.; Farley, K.; Flesch, G. J.; Francois, P.; Gellert, R.; Grant, J. A.; Grotzinger, J. P.; Gupta, S.; Herkenhoff, K. E.; Hurowitz, J. A.; Leshin, L. A.; Lewis, K. W.; McLennan, S. M.; Miller, K. E.; Moersch, J.; Morris, R. V.; Navarro-González, R.; Pavlov, A. A.; Perrett, G. M.; Pradler, I.; Squyres, S. W.; Summons, R. E.; Steele, A.; Stolper, E. M.; Sumner, D. Y.; Szopa, C.; Teinturier, S.; Trainer, M. G.; Treiman, A. H.; Vaniman, D. T.; Vasavada, A. R.; Webster, C. R.; Wray, J. J.; Yingst, R. A. Volatile and organic compositions of sedimentary rocks in Yellowknife Bay, Gale Crater, Mars. *Science* **2014**, *343*, 1245267.
- (9) Kim, Y. S.; Wo, K. P.; Maity, S.; Atreya, S. K.; Kaiser, R. I. Radiation-induced formation of chlorine oxides and their potential role in the origin of Martian perchlorates. *J. Am. Chem. Soc.* **2013**, *135*, 4910–4913.
- (10) Clark, B. C.; Kounaves, S. P. Evidence for the distribution of perchlorates on Mars. *Int. J. Astrobiol.* **2016**, *15*, 311–318.
- (11) Jackson, W. A.; Davila, A. F.; Sears, D. W. G.; Coates, J. D.; McKay, C. P.; Brundrett, M.; Estrada, N.; Böhlke, J. K. Widespread occurrence of (per)chlorate in the Solar System. *Earth Planet. Sci. Lett.* **2015**, *430*, 470–476.
- (12) Kounaves, S. P.; Carrier, B. L.; O'Neil, G. D.; Stroble, S. T.; Claire, M. W. Evidence of martian perchlorate, chlorate, and nitrate in Mars meteorite EETA79001: Implications for oxidants and organics. *Icarus* **2014**, *229*, 206–213.
- (13) Youngblut, M. D.; Wang, O.; Barnum, T. P.; Coates, J. D. (Per)chlorate in biology on earth and beyond. *Annu. Rev. Microbiol.* **2016**, *70*, 435–457.
- (14) Davila, A. F.; Willson, D.; Coates, J. D.; McKay, C. P. Perchlorate on Mars: A chemical hazard and a resource for humans. *Int. J. Astrobiol.* **2013**, *12*, 321–325.
- (15) Youngblut, M. D.; Tsai, C.-L.; Clark, I. C.; Carlson, H. K.; Maglaqui, A. P.; Gau-Pan, P. S.; Redford, S. A.; Wong, A.; Tainer, J. A.; Coates, J. D. Perchlorate reductase is distinguished by active site aromatic gate residues. *J. Biol. Chem.* **2016**, *291*, 9190–9202.
- (16) Schwarz, G.; Mendel, R. R.; Ribbe, M. W. Molybdenum cofactors, enzymes and pathways. *Nature* **2009**, *460*, 839–847.
- (17) Bertero, M. G.; Rothery, R. A.; Palak, M.; Hou, C.; Lim, D.; Blasco, F.; Weiner, J. H.; Strynadka, N. C. J. Insights into the respiratory electron transfer pathway from the structure of nitrate reductase A. *Nat. Struct. Mol. Biol.* **2003**, *10*, 681–687.
- (18) Jormakka, M.; Törnroth, S.; Byrne, B.; Iwata, S. Molecular basis of proton motive force generation: Structure of formate dehydrogenase-N. *Science* **2002**, *295*, 1863–1868.
- (19) Hofbauer, S.; Gruber, C.; Pirker, K. F.; Sündermann, A.; Schaffner, I.; Jakopitsch, C.; Oostenbrink, C.; Furtmüller, P. G.; Obinger, C. Transiently produced hypochlorite is responsible for the irreversible inhibition of chlorite dismutase. *Biochemistry* **2014**, *53*, 3145–3157.
- (20) De Geus, D. C.; Thomassen, E. A. J.; Hagedoorn, P.-L.; Pannu, N. S.; van Duijn, E.; Abrahams, J. P. Crystal structure of chlorite dismutase, a detoxifying enzyme producing molecular oxygen. *J. Mol. Biol.* **2009**, *387*, 192–206.
- (21) Melnyk, R. A.; Youngblut, M. D.; Clark, I. C.; Carlson, H. K.; Wetmore, K. M.; Price, M. N.; Iavarone, A. T.; Deutschbauer, A. M.; Arkin, A. P.; Coates, J. D. Novel mechanism for scavenging of hypochlorite involving a periplasmic methionine-rich peptide and methionine sulfoxide reductase. *mBio* **2015**, *6*, No. e00233-15.
- (22) Lee, C. C.; Sickerman, N. S.; Hu, Y.; Ribbe, M. W. YedY: A mononuclear molybdenum enzyme with a redox-active ligand? *ChemBioChem* **2016**, *17*, 453–455.
- (23) Coates, J. D.; Achenbach, L. A. Microbial perchlorate reduction: Rocket-fuelled metabolism. *Nat. Rev. Microbiol.* **2004**, *2*, 569–580.
- (24) Ford, C. L.; Park, Y. J.; Matson, E. M.; Gordon, Z.; Fout, A. R. A bioinspired iron catalyst for nitrate and perchlorate reduction. *Science* **2016**, *354*, 741–743.
- (25) Drummond, M. J.; Miller, T. J.; Ford, C. L.; Fout, A. R. Catalytic perchlorate reduction using iron: Mechanistic insights and improved catalyst turnover. *ACS Catal.* **2020**, *10*, 3175–3182.
- (26) Abu-Omar, M. M.; McPherson, L. D.; Arias, J.; Béreau, V. M. Clean and efficient catalytic reduction of perchlorate. *Angew. Chem., Int. Ed.* **2000**, *39*, 4310–4313.
- (27) Liu, J.; Wu, D.; Su, X.; Han, M.; Kimura, S. Y.; Gray, D. L.; Shapley, J. R.; Abu-Omar, M. M.; Werth, C. J.; Strathmann, T. J. Configuration control in the synthesis of homo- and heteroleptic bis(oxazolonylphenolato/thiazolonylphenolato) chelate ligand complexes of oxorhenium(V): Isomer effect on ancillary ligand exchange dynamics and implications for perchlorate reduction catalysis. *Inorg. Chem.* **2016**, *55*, 2597–2611.
- (28) Liu, J.; Choe, J. K.; Wang, Y.; Shapley, J. R.; Werth, C. J.; Strathmann, T. J. Bioinspired complex-nanoparticle hybrid catalyst system for aqueous perchlorate reduction: Rhenium speciation and its influence on catalyst activity. *ACS Catal.* **2015**, *5*, 511–522.
- (29) Elrod, L. T.; Kim, E. Lewis acid assisted nitrate reduction with biomimetic molybdenum oxotransferase complex. *Inorg. Chem.* **2018**, *57*, 2594–2602.
- (30) Jiang, J.; Holm, R. H. Reaction systems related to dissimilatory nitrate reductase: Nitrate reduction mediated by bis(dithiolene) tungsten complexes. *Inorg. Chem.* **2005**, *44*, 1068–1072.
- (31) Liu, J.; Chen, X.; Wang, Y.; Strathmann, T. J.; Werth, C. J. Mechanism and mitigation of the decomposition of an oxorhenium complex-based heterogeneous catalyst for perchlorate reduction in water. *Environ. Sci. Technol.* **2015**, *49*, 12932–12940.
- (32) Bergeron, R. J. Synthesis and solution structure of microbial siderophores. *Chem. Rev.* **1984**, *84*, 587–602.
- (33) Liu, J.; Su, X.; Han, M.; Wu, D.; Gray, D. L.; Shapley, J. R.; Werth, C. J.; Strathmann, T. J. Ligand design for isomer-selective oxorhenium(V) complex synthesis. *Inorg. Chem.* **2017**, *56*, 1757–1769.
- (34) Hurley, K. D.; Zhang, Y.; Shapley, J. R. Ligand-enhanced reduction of perchlorate in water with heterogeneous Re–Pd/C catalysts. *J. Am. Chem. Soc.* **2009**, *131*, 14172–14173.
- (35) Liu, B. Y.; Wagner, P. A.; Earley, J. E. Reduction of perchlorate ion by (N-(hydroxyethyl)ethylenediaminetriacetato) aquatitanium(III). *Inorg. Chem.* **1984**, *23*, 3418–3420.
- (36) Liu, J.; Han, M.; Wu, D.; Chen, X.; Choe, J. K.; Werth, C. J.; Strathmann, T. J. A new bioinspired perchlorate reduction catalyst with significantly enhanced stability via rational tuning of rhenium coordination chemistry and heterogeneous reaction pathway. *Environ. Sci. Technol.* **2016**, *50*, 5874–5881.
- (37) Hurley, K. D.; Shapley, J. R. Efficient heterogeneous catalytic reduction of perchlorate in water. *Environ. Sci. Technol.* **2007**, *41*, 2044–2049.
- (38) Cao, J.; Elliott, D.; Zhang, W.-X. Perchlorate reduction by nanoscale iron particles. *J. Nanopart. Res.* **2005**, *7*, 499–506.

- (39) Xiong, Z.; Zhao, D.; Pan, G. Rapid and complete destruction of perchlorate in water and ion-exchange brine using stabilized zero-valent iron nanoparticles. *Water Res.* **2007**, *41*, 3497–3505.
- (40) Moore, A. M.; De Leon, C. H.; Young, T. M. Rate and extent of aqueous perchlorate removal by iron surfaces. *Environ. Sci. Technol.* **2003**, *37*, 3189–3198.
- (41) Hori, H.; Sakamoto, T.; Tanabe, T.; Kasuya, M.; Chino, A.; Wu, Q.; Kannan, K. Metal-induced decomposition of perchlorate in pressurized hot water. *Chemosphere* **2012**, *89*, 737–742.
- (42) Hori, H.; Kamijo, A.; Inoue, M.; Chino, A.; Wu, Q.; Kannan, K. Efficient decomposition of perchlorate to chloride ions in subcritical water by use of steel slag. *Environ. Sci. Pollut. Res.* **2018**, *25*, 7262–7270.
- (43) Gu, B.; Dong, W.; Brown, G. M.; Cole, D. R. Complete degradation of perchlorate in ferric chloride and hydrochloric acid under controlled temperature and pressure. *Environ. Sci. Technol.* **2003**, *37*, 2291–2295.
- (44) Wang, C.; Huang, Z.; Lippincott, L.; Meng, X. Rapid Ti(III) reduction of perchlorate in the presence of β -alanine: Kinetics, pH effect, complex formation, and β -alanine effect. *J. Hazard. Mater.* **2010**, *175*, 159–164.
- (45) McPherson, L. D.; Drees, M.; Khan, S. I.; Strassner, T.; Abu-Omar, M. M. Multielectron atom transfer reactions of perchlorate and other substrates catalyzed by rhenium oxazoline and thiazoline complexes: Reaction kinetics, mechanisms, and density functional theory calculations. *Inorg. Chem.* **2004**, *43*, 4036–4050.
- (46) Liu, J.; Choe, J. K.; Sasnow, Z.; Werth, C. J.; Strathmann, T. J. Application of a Re–Pd bimetallic catalyst for treatment of perchlorate in waste ion-exchange regenerant brine. *Water Res.* **2013**, *47*, 91–101.
- (47) Choe, J. K.; Boyanov, M. I.; Liu, J.; Kemner, K. M.; Werth, C. J.; Strathmann, T. J. X-ray spectroscopic characterization of immobilized rhenium species in hydrated rhenium-palladium bimetallic catalysts used for perchlorate water treatment. *J. Phys. Chem. C* **2014**, *118*, 11666–11676.
- (48) Choe, J. K.; Shapley, J. R.; Strathmann, T. J.; Werth, C. J. Influence of rhenium speciation on the stability and activity of Re/Pd bimetal catalysts used for perchlorate reduction. *Environ. Sci. Technol.* **2010**, *44*, 4716–4721.
- (49) Greiner, M. T.; Rocha, T. C.; Johnson, B.; Klyushin, A.; Knop-Gericke, A.; Schlögl, R. The oxidation of rhenium and identification of rhenium oxides during catalytic partial oxidation of ethylene: An in-situ XPS study. *Z. Phys. Chem.* **2014**, *228*, 521–541.
- (50) Deshwal, B. R.; Jo, H. D.; Lee, H. K. Reaction kinetics of decomposition of acidic sodium chlorite. *Can. J. Chem. Eng.* **2004**, *82*, 619–623.
- (51) Lippert, C. A.; Arnstein, S. A.; Sherrill, C. D.; Soper, J. D. Redox-active ligands facilitate bimetallic O₂ homolysis at five-coordinate oxorhenium(V) centers. *J. Am. Chem. Soc.* **2010**, *132*, 3879–3892.
- (52) Arias, J.; Newlands, C. R.; Abu-Omar, M. M. Kinetics and mechanisms of catalytic oxygen atom transfer with oxorhenium(V) oxazoline complexes. *Inorg. Chem.* **2001**, *40*, 2185–2192.
- (53) Rundlöf, T.; Mathiasson, M.; Bekiroglu, S.; Hakkarainen, B.; Bowden, T.; Arvidsson, T. Survey and qualification of internal standards for quantification by ¹H NMR spectroscopy. *J. Pharm. Biomed. Anal.* **2010**, *52*, 645–651.
- (54) Polshin, V.; Popescu, D.-L.; Fischer, A.; Chanda, A.; Horner, D. C.; Beach, E. S.; Henry, J.; Qian, Y.-L.; Horwitz, C. P.; Lente, G.; Fabian, I.; Münck, E.; Bominaar, E. L.; Ryabov, A. D.; Collins, T. J. Attaining control by design over the hydrolytic stability of Fe-TAML oxidation catalysts. *J. Am. Chem. Soc.* **2008**, *130*, 4497–4506.
- (55) Ghosh, A.; Ryabov, A. D.; Mayer, S. M.; Horner, D. C.; Prasuhn, D. E.; Sen Gupta, S.; Vuocolo, L.; Culver, C.; Hendrich, M. P.; Rickard, C. E. F.; Norman, R. E.; Horwitz, C. P.; Collins, T. J. Understanding the mechanism of H⁺-induced demetalation as a design strategy for robust iron(III) peroxide-activating catalysts. *J. Am. Chem. Soc.* **2003**, *125*, 12378–12379.
- (56) Wähler, K.; Ludewig, A.; Szabo, P.; Harms, K.; Meggers, E. Rhenium complexes with red-light-induced anticancer activity. *Eur. J. Inorg. Chem.* **2014**, *2014*, 807–811.
- (57) Hasan, K.; Bansal, A. K.; Samuel, I. D.; Roldán-Carmona, C.; Bolink, H. J.; Zysman-Colman, E. Tuning the emission of cationic iridium(III) complexes towards the red through methoxy substitution of the cyclometalating ligand. *Sci. Rep.* **2015**, *5*, 12325.
- (58) Albert Cotton, F.; Wilkinson, G. *Advanced Inorganic Chemistry*; Wiley: New York, 1988; Vol. 5.